Projected Orbital Demand and LEO Environmental Capacity

Andrea D'Ambrosio,[*] Miles Lifson,[†] Daniel Jang,[‡] Celina Pasiecznik,[§] Richard Linares[¶]
Department of Aeronautics and Astronautics, Massachusetts Institute of Technology, 77 Massachusetts Ave., Cambridge, MA 02139, USA

ABSTRACT

A large number of spacecraft have been proposed for launch into Low Earth Orbit (LEO) over the next decade, leading to a significant increase in the LEO anthropogenic space object population. This implicates important concerns regarding space sustainability and LEO orbital capacity. The aim of this paper is to estimate the benefits of orbital slotting for LEO orbital capacity. This is carried out in two steps. The first step considers the intrinsic capacity of active spacecraft, based on an orbital slotting model and a non-conjunction requirement for active on-station spacecraft. Current and future proposed constellations are evaluated for overlaps in orbital altitude based on various assumptions. The results of this analysis are then used for a second step, where the long-term LEO evolution is estimated through a multi-species multi-bin source sink evolutionary model. The model features several species per shell including active on-station satellites, unslotted satellites, derelict satellites and debris. Several fluxes of incoming and outgoing objects are evaluated, taking into account new launches, the atmospheric drag effects, collisions, and post-mission disposal. An optimization approach is used to compute the LEO orbital capacity while satisfying some imposed constraints, such as the intrinsic capacity and the sustainability constraints. Benefits of slotting for different levels of collision avoidance efficacy and post-mission disposal compliance are estimated for initial conditions reflecting today's trackable LEO population and for those assuming the presence of most large constellations filed with the International Telecommunications Union. In both scenarios, slotting improves capacity, but the effect size is small especially for good collision avoidance efficacy, likely due to the sustainability constraint already significantly limiting traffic at higher altitudes. For active on active collision avoidance failure rates of approximately 10^{-4} and higher, slotting appears to significantly reduce the number of satellites destroyed by active on active collisions, providing significant logistical and economic benefits. Future work is proposed to better understand these results and to verify the utilized model against other modeling methodologies.

1. INTRODUCTION

Numerous large constellations have been proposed in recent years. If even half of the planned Large LEO Constellations (LLCs) make it to orbit, the projected number of satellites in Low Earth Orbit (LEO) will increase by an order of magnitude over the next decade. Debris in the LEO region is governed by uncertain inputs and behaviors that make it very challenging to accurate predict the long-term response of the environment with sufficient accuracy and precision to inform decision-making. Such factors include spacecraft post-mission disposal rates, solar weather and coupled levels of atmospheric drag, non-linear spacecraft dynamics, epistemic uncertainty concerning the distribution and quantity of sub-trackable lethal debris, and the inherently difficulty associated with projecting future LEO orbital demand and use.

At the same time, there is increasing interest in such projections because of fears that impending growth in the active satellite population may be unsustainable and lead to degradation of the LEO environment, absent significant changes to best practices for debris mitigation and associated operational and regulatory practices. Tools to model the evolution of the space environment can help assess the efficacy of various mitigation and remediation efforts, inform policy and

[*]Postdoctoral Associate, Department of Aeronautics and Astronautics. E-mail: andreada@mit.edu
[†]Ph.D. Candidate, Department of Aeronautics and Astronautics. E-mail: mlifson@mit.edu
[‡]Ph.D. Candidate, Department of Aeronautics and Astronautics, E-mail: djang@mit.edu
[§]SM Candidate, Department of Aeronautics and Astronautics. E-mail: cpasiecz@mit.edu
[¶]Rockwell International Career Development Professor, Associate Professor of Aeronautics and Astronautics, Department of Aeronautics and Astronautics. E-mail: linaresr@mit.edu

regulatory decision-making, and inform the development for future space systems. These benefits grow substantially if physics and engineering models can be integrated with economic and behavioral models to include how agents iteratively response to changes to the space environment.

The work in this paper marries two streams of thinking related to LEO orbital capacity. The first stream considers the number of on-station spacecraft that may be admitted by a certain orbital configuration subject to minimum separations between spacecraft at point of closest approach using periodic reference orbits. This constraint is known as the intrinsic capacity of slotted spacecraft and is described further in [1, 2] and associated works. The second stream assesses risk-based capacity, the capacity subject to collisions, drag, and other notable phenomena, using a source-sink evolutionary model (SSEM) to model evolution of LEO populations of various types of objects and calculate LEO environmental capacity. This work is described further in [3, 4] and builds on a long stream of work using SSEMs for evolutionary orbital modeling. SSEMs, also referred to as Particle-in-a-box models, are based on systems of coupled Ordinary Differential Equations (ODEs), which describe the time evolution of different species of anthropogenic space objects (ASOs). In these models, the main sources and the sinks of each species are considered together with the main interactions occurring among them. Key papers using SSEMs include the Kessler and Cour-Palais's original paper identifying the "Kessler Syndrome" [5] along with updates in [6, 7]; work by Talent [8] and Somma [9] on SSEM model development; and papers applying SSEMs to assess techniques for mitigation and remediation or environmental capacity [10, 11].

Efforts to describe and integrate the two approaches are presented in [12, 13]. Here, these methods are used to perform a sensitivity study on LEO orbital capacity for various levels of collision avoidance efficacy between active spacecraft and rates of post-mission disposal. This is combined with a new survey of currently planned LLCs, which is used to provide a baseline to evaluate remaining orbital capacity.

This manuscript is organized as follows:

- Section 1 introduces the problem, literature review and motivation for this work.
- Section 2 lists current and planned constellations identified for LEO, finds overlaps in orbital altitude based on both nominal altitude and assuming constellations employ J2/J3 frozen orbits, and generates a baseline demand curve used to anchor future capacity estimation work in the paper.
- Section 3 describes the MOCAT-4S model and utilized modeling constraints.
- Section 4 explains the methodology behind calculation of LEO capacity.
- Section 5 shows the results from the numerical simulations using MOCAT-4S at various levels of collision avoidance efficacy and post-mission disposal.
- Section 6 summarizes the conclusions of the work.

2. CURRENT ORBITAL DEMAND AND ORBITAL OVERLAPS

Future LLC orbital demand is large, but uncertain. To help generate a future maximalist demand case to assess the benefits of slotting, a set of future LEO satellite data was gathered from International Telecommunications Union Coordination Request and Advance Publication Information filings from 2017 to present. The extremely large filings from Rwanda were excluded. This dataset was provided by [14]. As seen in Fig. 1, there is considerable demand in the modeled region of LEO across a variety of inclinations. However, 94.7% of satellites belong to shells of 100 or more satellites each in near-circular orbits. In this figure no attempt was made to filter duplications between Coordination Request and Advance Publication Information filings or to remove previous versions of updated filings.

While ITU filings contain nominal apogee, perigee, semi-major axis, and eccentricity information, data for LLCs almost all claim perfectly circular orbits. In practice, these constellations will likely use small but non-zero eccentricity to help counteract secular element drifts due to non-spherical Earth effects. Depending on altitude and inclination, these effects can spread a constellation across 15 km of altitude or more, with greater altitude range for constellations with inclinations closer to 90 deg.

To better model these constellations and their altitude distributions, a single satellite was modeled per filings, with a J_2/J_3 frozen orbit featuring an argument of perigee of 90 deg set such that its equatorial crossing occurs at the nominal

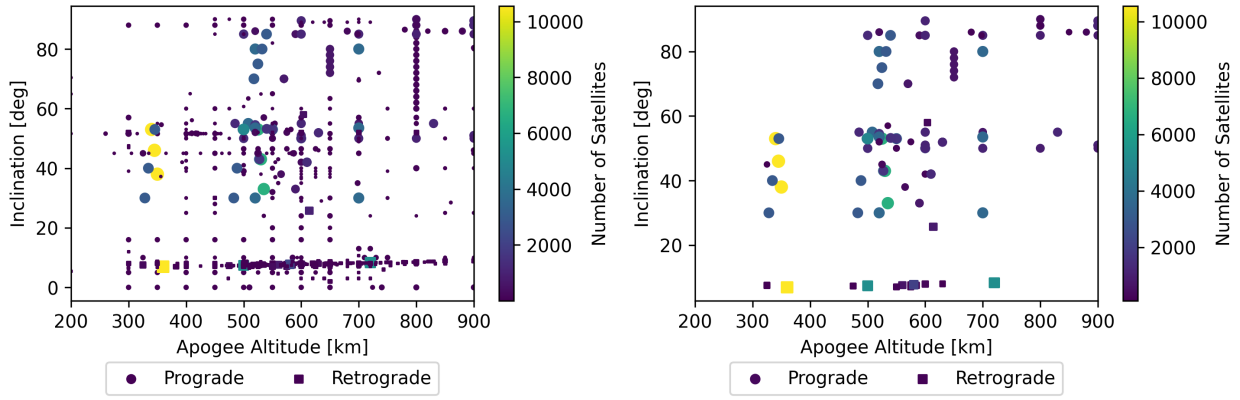

(a) All filings.

(b) Shells $\geq$ 100 satellites.

Fig. 1: LLC demand in ITU Coordination Request and Advance Publication Information Filings $<$ 900 km apogee and excluding Rwandan LLCs.

altitude provided in ITU filings. This satellite was then propagated for an orbital period under a J_3 model to compute the distribution of altitude as a function of time over the orbital period. This altitude-time density curve was then scaled such that the area under the curve calculated with the trapezoidal rule was equivalent to the number of satellites in the filed shell. The resultant satellite density curves can then be integrated within each altitude bin of the model to create bin-discretized satellite density equations.

A list of the shells used is included in Table 5 in the Appendix. Here, clear duplicates or older versions of updated filings were omitted, erring on the side of including additional shells in the case of uncertainty. Note that this table includes some constellations which may not feature propulsion, meaning their inclusion under a slotting assumption is an over-estimate.

Fig. 2 shows the difference between satellite altitude density based on the nominal ITU altitudes and the method described in this section. As seen in this figure, the calculation method distributes satellites more evenly across a credible altitude range, limiting the sharp spikes between bins seen in the nominal case, and inaccuracies caused by constellations near bin border transitions. This process is described in more detail in [13].

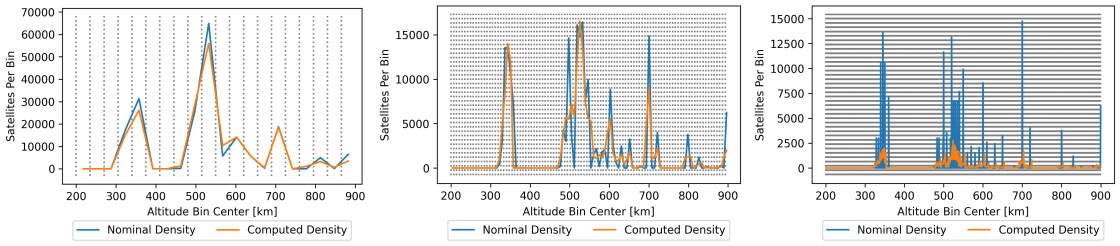

(a) 20 Bins.

(b) 100 Bins.

(c) 1000 Bins.

Fig. 2: Calculating satellite distributions for shells in Table 5 reduces nominal peaks and may shift populations significantly if they cross a bin boundary.

3. MOCAT-4S SOURCE-SINK MODEL

To study the temporal evolution of ASOs during time, a multi-bin multi-species source-sink model, called MOCAT-4S and belonging to the MIT Orbital Capacity Assessment Tool (MOCAT), is employed. A brief description of the model and the main interactions are presented in this section together with the system of ODEs describing the model. However, for the sake of conciseness, the full derivation of MOCAT-4S is not reported here and can be

found in [13]. The MOCAT-4S extends the baseline model MOCAT-3 [3], where three species were considered. MOCAT-4S includes four different species: slotted satellites (S), unslotted satellites (S_u), derelict satellites (D), and debris (N). Slotted spacecraft indicate on-station spacecraft station-keeping to maintain position within slots within near-circular compatible shells, whereas unslotted spacecraft indicates satellites not designed to feature compatible orbits. Derelict satellites represent intact satellites that fail to meet the post-mission disposal guidelines and remain on-orbit, but without the ability to perform collision avoidance maneuvers. The qualitative scheme showing the modeled phenomena within the MOCAT-4S is illustrated in Fig. 3. The system of ODEs describing the MOCAT-4S model is

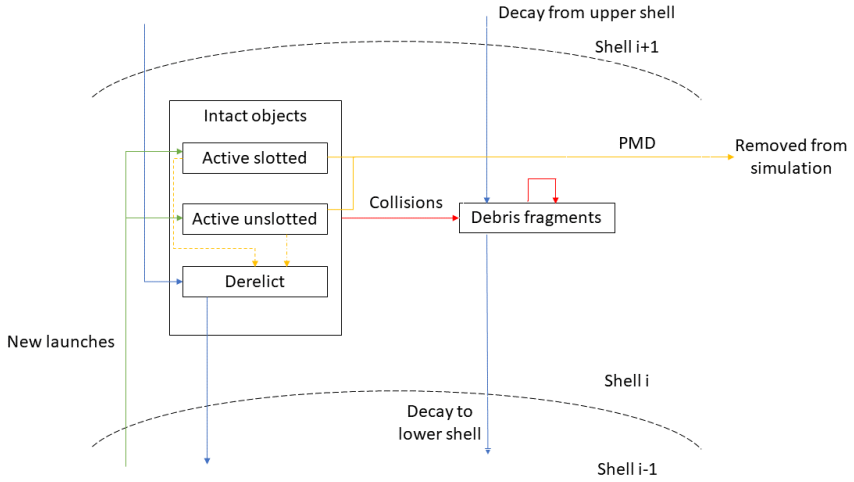

Fig. 3: Schematics of the MOCAT-4S source-sink model.

provided by:

$$\dot{\boldsymbol{P}} = \dot{\boldsymbol{\Lambda}} + \dot{\boldsymbol{C}}_{PMD} + \dot{\boldsymbol{F}} + \dot{\boldsymbol{C}} \tag{1}$$

where each term is meant to be function of time and altitude. In particular, $\boldsymbol{P}(h,t) = [S(h,t), D(h,t), N(h,t), S_u(h,t)]$ refers to entire population vector, considering all the species, in the h-th shell at time instant t. The other terms are:

- $\dot{\boldsymbol{\Lambda}} = [\lambda_s, 0, 0, \lambda_u]$ is the launch rate (usually represented by the number of objects launched per year);
- $\dot{\boldsymbol{C}}_{PMD}$ is the term related to the post-mission disposal, occurring with a probability of success P_M after Δt years of operational life.

$$\dot{\boldsymbol{C}}_{PMD} = \left[-\frac{S}{\Delta t}, +\frac{(1-P_M)(S+S_u)}{\Delta t}, 0, -\frac{S_u}{\Delta t} \right] \tag{2}$$

- $\dot{\boldsymbol{F}}$ is the term related to the atmospheric drag orbital decay effect. Active satellites (both slotted and unslotted) are assumed not to be subject to the decay effects since they can perform station-keeping maneuvers to remain in their orbit. Therefore, only derelicts and debris experience the orbital decay effects.

$$\dot{\boldsymbol{F}} = \left[0, \dot{F}_{d,D}, \dot{F}_{d,N}, 0 \right] \tag{3}$$

Indicating with Q the number of objects belonging to a generic species, $\dot{F}_{d,Q}$ can be written as follows:

$$\dot{F}_{d,Q} = -\frac{Q_+ v_+}{d} + \frac{Q v}{d} \tag{4}$$

where d is the thickness of the shell, and the subscript + refers to the quantities related to the shell right above the current one. v is the rate of change of the semi-major axis, expressed as:

$$v = -\rho B \sqrt{\mu R} \tag{5}$$

In Eq. (5), $\mu = 398601$ km^3/s^2 is the Earth gravitational parameter; R is the radial distance of the objects with respect to the center of the Earth (the assumption of near-circular orbits is here carried out, such that the semi-major axis corresponds to the radial distance); $B = c_D \frac{A}{m}$ is related to the ballistic coefficient with $c_D = 2.2$, A, and m being the drag coefficient, the area and the mass of the object, respectively; and ρ is the atmospheric density, computed as a static exponential model obtained combining the U.S. Standard Atmosphere and the CIRA-72 model,

$$\rho = \rho_0 \exp\left(-\frac{h-h_0}{H}\right) \tag{6}$$

where h is the altitude of the object, ρ_0 is the atmospheric density at reference altitude h_0, and H is the scale height. The values of ρ_0, h_0, and H can be found in Table 8-4 of [15].

- $\dot{\boldsymbol{C}}$ expresses the contributions due to the collisions among the species of ASOs.

$$\dot{\boldsymbol{C}} = [\dot{C}_S, \dot{C}_D, \dot{C}_N \cdot n_f, \dot{C}_{S_u}] \tag{7}$$

The number of fragments n_f generated by the collisions can be estimated considering the NASA standard break-up model [16]. Two types of collisions are taken into account: catastrophic ($n_{f,c}$) and non-catastrophic or damaging ($n_{f,nc}$) collision. For simplicity, in this work, collisions are considered catastrophic between intact objects, whereas they are non-catastrophic when debris are involved.

$$n_{f,c} = 0.1\, L_C^{-1.71} (M_i + M_j)^{0.75} \tag{8}$$

$$n_{f,nc} = 0.1\, L_C^{-1.71} (M_p \cdot v_{imp}^2)^{0.75} \tag{9}$$

where $M_{i/j}$ is the mass associated to the species i/j, M_p is the mass of the projectile (i.e., the mass of the less massive object, $M_p = \min(M_i, M_j)$), L_C is the characteristic length (assumed to be 0.1 m), and v_{imp} is the impact velocity (assumed to be equal to 10 km/s). The generic term $\dot{C}_i$ is provided as follows:

$$\dot{C}_i = \sum_{j=1}^{N_s} \Gamma_{ij} \phi_{ij} Q_i Q_j + \dot{C}_{i,add} \tag{10}$$

where N_s is the number of species considered (in this work $N_s = 4$), $i, j = 1, ..., N_s$ are the subscripts indicating each generic species Q, and Γ_{ij} are the components of the following matrix:

$$\Gamma = \begin{bmatrix} -(1-\zeta)\alpha_a & -(\delta+\alpha) & -(\delta+\alpha) & -\alpha_a \frac{S}{S+S_u} \\ +\delta & -1 & -1 & +\delta \\ +\alpha & +1 & +1 & +\alpha \\ -\alpha_a \frac{S_u}{S+S_u} & -(\delta+\alpha) & -(\delta+\alpha) & -\alpha_a \end{bmatrix} \tag{11}$$

In particular, δ represents the ratio of the density of disabling to lethal debris (δ takes into account that a collision generates both derelicts and debris), $(1-\zeta)$ represents the proportion of conjunctions between pairs of slotted spacecraft that are mitigated by the slotting system, with ζ being the slotting effectiveness coefficient. Because the proposed slotting system is intended to fully eliminate conjunction risk, ζ is set to 1, although alternative slotting systems that reduce but do not eliminate on-station collision risk are possible, α is the fraction of active versus inactive objects collisions that a satellite fails to avoid, α_a is the fraction of active versus active objects collisions that a satellite fails to avoid. In the case of collisions among active satellites, both the objects colliding are able to perform collision avoidance maneuvers; for this reason, $\alpha_a < \alpha$. Finally, ϕ_{ij} is related to the intrinsic probability of collision and it can be expressed as [10]:

$$\phi_{ij} = \pi \frac{v_r(h)(r_i + r_j)^2}{V(h)} \tag{12}$$

where $v_r(h)$ represents the relative impact velocity, in this work assumed to be constant and equal to 10 km/s, $V(h)$ is the volume of the orbital shell, and $r_{i,j}$ is the radius of the object.

All the interactions of the MOCAT-4S model are summarized in Table 1, where each row reports all the terms to sum in order to obtain the expression of the time derivatives of all the species ($\dot{S}$, $\dot{D}$, $\dot{N}$, and $\dot{S}_u$).

Table 1: Interactions among the species of the MOCAT-4S model.

	Species	S (Slotted satellites)	D (Derelicts)	N (Debris)	S_u (Unslotted satellites)
$\dot{\Lambda}$ New Launches	-	λ_s	0	0	λ_u
$\dot{C}_{PMD}$ Post-Mission Disposal	-	$-\frac{S}{\Delta t}$	$\frac{(1-P_M)(S+S_u)}{\Delta t}$	0	$-\frac{S_u}{\Delta t}$
$\dot{F}$ Drag	-	0	$\dot{F}_{d,D}$	$\dot{F}_{d,N}$	0
$\dot{C}$ Collision Source	S	$-(1-\zeta)\alpha_a\phi_{1,1}S^2$	$\phi_{1,2}\delta DS$ $+\phi_{1,3}\delta NS$	$n_{f,13}\phi_{1,3}\alpha SN$ $+n_{f,12}\phi_{1,2}\alpha SD$ $+(1-\zeta)n_{f,11}\alpha_a\phi_{1,1}S^2$ $+n_{f,14}\alpha_a\phi_{1,4}SS_u$	$-\alpha_a\phi_{1,4}\frac{SS_u^2}{S+S_u}$
	D	$-\phi_{1,2}(\delta+\alpha)SD$	$-\phi_{2,2}D^2$	$n_{f,22}\phi_{2,2}D^2$ $+\phi_{2,3}n_{f,23}DN$	$-\phi_{4,2}(\delta+\alpha)S_uD$
	N	$-\phi_{1,3}(\delta+\alpha)SN$	$-\phi_{2,3}DN$	$n_{f,33}\phi_{3,3}N^2$	$-\phi_{4,3}(\delta+\alpha)S_uN$
	S_u	$-\alpha_a\phi_{1,4}\frac{S_uS^2}{S+S_u}$	$\phi_{4,2}\delta DS_u$ $+\phi_{4,3}\delta NS_u$	$n_{f,43}\phi_{4,3}\alpha S_uN$ $+n_{f,42}\phi_{4,2}\alpha S_uD$ $+n_{f,44}\alpha_a\phi_{4,4}S_u^2$	$-\alpha_a\phi_{4,4}S_u^2$

4. MAXIMUM LEO ORBITAL CAPACITY

Calculation of maximum LEO environmental capacity is of interest to regulators and many other stakeholders. In this work, orbital capacity is defined as the number of satellites that may be admitted to LEO subject to various sustainability constraints. Maximum LEO orbital capacity is calculated as a constrained optimization problem. The goal is to maximize the number of satellites residing in LEO at the end of the propagation time of the analysis, while fulfilling some imposed constraints, such as the sustainability constraint, which limits the growth of the space debris population, and the intrinsic capacity constraint, which poses a maximum bound on the satellites per altitude bin. By following this approach, the optimization variables are the launch rate of active satellites per altitude bin (both slotted and unslotted). The optimization is carried out via the metaheuristics Particle Swarm Optimization (PSO) algorithm. The augmented cost function, incorporating penalty terms related to the constraints, can be written as follows:

$$J = \frac{\beta_0}{S_{f,tot}} + \sum_{q=1}^{N_{con}} \beta_q \Phi_q \tag{13}$$

where $S_{f,tot}$ represents the total number of satellites at the end of the propagation period considering all the altitude bins, N_{con} is the number of constraints, Φ_q is a term related to the generic constraint to satisfy, β_0 and β_q are the constant non-negative coefficients that weight the terms in the cost function. In particular, β_q is always null when the corresponding constraint is fulfilled.

1. **Final time constraint.** Due to the sensitivity of the model to the launch rate, a very high launch rate may lead to numerical overflow during the simulation period. Therefore, a constraint is required to penalize those solutions for which the desired final time of the simulation is not reached. Hence,

$$\Phi_1 = t_{f,d} - t_f, \qquad \beta_1 = 10^9 \tag{14}$$

2. **Sustainability constraint.** To ensure space remains usable in the future, debris volumes should remain bounded and at tolerable levels. To represent this goal, a constraint on the derivative of the debris species at final time along each altitude bin should be imposed.[1] The ideal solution would be a negative derivative of the debris

[1] In the model, compliant solutions tend to approach steady-state long-term behavior. The method used here potentially penalizes bounded but cyclic solutions and does not directly consider whether the stable debris population is consistent with an acceptable amount of risk to active spacecraft. While this constraint was adequate to produce reasonable solutions in this work, more sophisticated definitions of a stability constraint could and should be considered where indicated.

population, which would indicate a decreasing trend. However, this is not an easy condition to satisfy during the optimization. For this reason, a small positive tolerance on the derivative is permitted to obtain better convergence of the algorithm, while maintaining acceptably low levels of debris growth. For altitude bins where this tolerance $\bar{\dot{N}}_h$ is exceeded (i.e., when $\dot{N}_h > \bar{\dot{N}}_h$), the following penalty function is computed and added to the cost function:

$$\Phi_2 = \sum_{h=1}^{N_{bins}} \dot{N}_h, \qquad \beta_3 = 100 \tag{15}$$

3. **Slotted/unslotted satellite ratio constraint.** While LLCs will produce most future demand, there will also be non-constellation traffic and some spacecraft which cannot or will not use slotted compatible orbits. For this reason, it remains necessary to model the launch of new unslotted satellites, as a percentage (θ_{S,S_u}) of the slotted population. Two different approaches could be employed to control the ratio of slotted to unslotted satellites. The first approach considers the launch rate per bin for slotted satellites as the only optimization variables ($\lambda_s(h)$) while the launch rate of unslotted satellites is considered to be $\lambda_u(h) = \theta_{S,S_u}\lambda_s(h)$. On the other hand, the second approach independently considers the launch rates of both slotted and unslotted spacecraft per bin ($\lambda_s(h)$ and $\lambda_u(h)$) as optimization variables, with a penalty term is added in the cost function to ensure that the number of unslotted spacecraft does not exceed a certain percentage (θ_{S,S_u}) of the slotted satellites population. Accordingly, the following penalty term is introduced if the number of unslotted satellites in each altitude bin at final time ($S_{u,f}(h)$) exceeds the percentage (θ_{S,S_u}) of the number of slotted satellites ($S_f(h)$):

$$\Phi_3 = \sum_{h=1}^{N_{bins}} (S_{u,f}(h) - \theta_{S,S_u} S_f(h)), \qquad \beta_4 = 10 \tag{16}$$

While the second approach could be more accurate and provides more freedom to the optimizer to place unslotted satellites, the first approach is computationally faster, due to fewer optimization variables (N_{bin} instead of $2N_{bin}$), and because it inherently satisfies the constraint of Eq. (16). In this paper, the first approach is used, leaving further analysis on the comparisons between the two approaches for future works.

4. **Intrinsic capacity constraint.**

The overwhelming majority of LLCss make use of near circular orbits. For a uniform circular constellation under Keplerian motion, the number of potential satellite locations that can be admitted without generating hazardous self-conjunctions for a given minimum separation distance and inclination can be found using the methods proposed by Arnas et al. [1, 17, 18, 19, 2]. Using the process from [18], it is possible to exhaustively consider all circular uniform Keplerian constellations and fit empirical power laws by finding the constants c and b in Eq. (17) in order to approximate (for a given inclination) the relation between number of satellites (N_{sat}) and minimum angular separation between satellites (γ).

$$\gamma = cN_{sat}^{b} \tag{17}$$

The number of concentric shells that can be admitted in a particular volume of space is complicated, depending on the mean eccentricity vector of each shell, which perturbations are modeled in shell design, and station-keeping, among other factors [12]. If, as a simplifying assumption, each shell is assumed to require a fixed amount of altitude, then the number of slotted satellites per altitude bin can be estimated by:

$$S_{int} = N_{sat}\frac{d}{\gamma_{km}} \tag{18}$$

where d is the thickness of the altitude bin (in km) and γ_{km} is the vertical separation distance (in km) between shell centers. Note that γ and γ_{km} may be set independently, taking the same or different values.

In [13], this method for computing intrinsic capacity was used to define a constraint for the maximum population of slotted satellites per altitude bin. Specifically, the number of slotted satellites in each altitude bin and for each time instant must never exceed S_{int}. When this constraint is violated, the following penalty term is computed:

$$\Phi_4 = \sum_{t=0}^{L}\sum_{h=1}^{N_{bins}} [(S_{h,t} - S_{int,h}) + L/t], \qquad \beta_2 = 1 \tag{19}$$

where L indicates the number of time steps, N_{bins} is the number of altitude bins, $S_{h,t}$ is the number of slotted satellites at a certain altitude shell and time instant, and $S_{int,h}$ is the maximum number of slotted satellites provided by the intrinsic capacity analysis (this last quantity is not time-dependent). As can be seen, when the constraint is violated, the presence of the difference term in the brackets penalizes the cost function with the same excess quantity for each shell, whereas the last term penalizes the time step when the constraint is violated. By doing so, the optimization algorithm is forced to prefer those solutions for which the constraint is violated towards the end of the propagation period rather than at the beginning, eventually steering the solution towards satisfying the constraint.

5. NUMERICAL RESULTS

Numerical results are presented in this section. The parameters employed within the MOCAT-4S to run the simulations are reported in Tables 2 and 3, where the average physical characteristics of ASOs are taken from [10]. The altitude range analyzed in this work is 200-900 km. Above approximately 900 km, the sink due to the atmospheric drag does not play a significant role; therefore, different approaches considering models with active debris removal in combination with new post-mission disposal guidelines would be required to maintain a sustainable space environment. The analyzed LEO region is divided into 20 altitude bin, each 35 km in altitude. The propagation time chosen for the analysis is 200 years. As a simplifying assumption, the model features no incoming flux of derelicts and debris into the highest shell from orbits above 900 km, i.e., $D_{N_{bins}+1} = 0$ and $N_{N_{bins}+1} = 0$.

To study the benefits of compatible orbital slotting, it is assumed that slotted satellites are capable of always performing successful station-keeping maneuvers. As a result, the slotting effectiveness coefficient ζ is set equal to 1, so that there are no collisions between pair of slotted satellites. For this analysis, the sustainability constraint is set to $\bar{N}_h = 20$, which means that no more than 20 debris per year per altitude bin may be created by collisions during the final time interval of the propagation. Moreover, the ratio of unslotted/slotted satellites launch rates has been set equal to $\theta_{S,S_u} = 0.1$, about half as slotted as the ITU data. For the intrinsic capacity constraint, a reference inclination of 45 degree and 5 km of curvilinear minimum separation distance are considered, leading to $b = -0.83$ and $c = 478.83$ for Eq. (17). Hence, the maximum number of slotted satellites allowed per altitude bin ($S_{int,h}$), retrieved by Eq. (18), is illustrated in Fig. 4.[1] The minimum separation distance used is not meant to be realistic, but rather as a test scenario to avoid overly constraining the problem. The initial population, shown in Fig. 5, was obtained from Two-Line Elements (TLEs) data from space-track.org[2], following the same assumptions as in [13].

Table 2: Parameters employed for the simulations.

h_{min}	h_{max}	N_{bins}	d	Δt	v_r	α	δ	ζ	c_D	L_C
200 km	900 km	20	35 km	5 years	10 km/s	0.2	10	1	2.2	0.1 m

Table 3: Average physical characteristics of the ASOs.

ASO	m [kg]	b [m]	A [m^2]
S (slotted satellites)	223	1.49	1.741
D (derelicts)	223	1.49	1.741
N (debris)	0.64	0.18	0.02
S_u (unslotted satellites)	223	1.49	1.741

The MOCAT-4S model was then used to generate preliminary estimates for the benefits of orbital slotting in terms of increases to the number of admissible LEO satellites and in terms of reduction to the number of active satellites lost to collisions as compared to a MOCAT-4S propagation with comparable species populations, but the slotting effectiveness parameter ζ set to 0 (all the satellites are considered unslotted). A sensitivity study was conducted for various levels of collision avoidance efficacy (α_a) and the post-mission disposal compliance (P_M). MOCAT-4S optimization runs were performed 3 times for each combination of α and P_M according to the discretization reported

[1] This quantity is extrapolated significantly outside the power law fit window, which ends at 10,000 satellites. Caution should be used if adopting these values for other applications.

[2] The full TLE catalog was downloaded from `space-track.org`, accessed on July 9th, 2022.

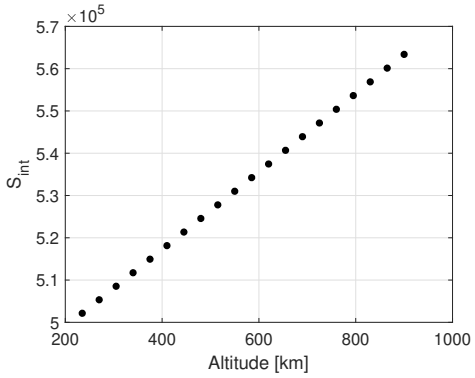

Fig. 4: Maximum number of slotted satellites.

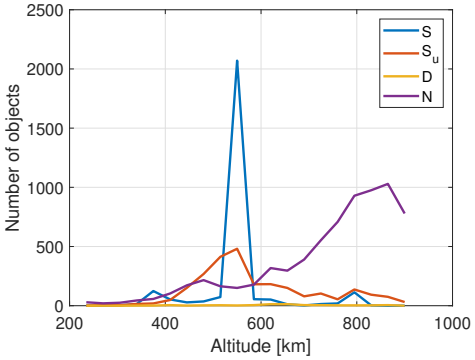

Fig. 5: TLE-derived Initial ASO Populations.

in Table 4. Error bars on figures refer to +/- one standard deviation among the results from the various optimization runs. No error bars were reported for changes to percentage capacity, as they involve the use of several terms that all vary differently. This optimization was performed using the MIT Supercloud [20].

Table 4: Discretization of α_a and P_M employed for the sensitivity analysis.

Parameter	Discretization
Collision avoidance failure (α_a)	$[10^{-6}, 10^{-5}, 10^{-4}, 10^{-3}, 10^{-2}, 10^{-1}]$
Post-mission disposal compliance level (P_M)	$[0.5, 0.6, 0.7, 0.8, 0.9, 0.95, 0.999]$

For the optimization procedure, $\beta_0 = 10^6$. The lower bound of the launch rate ($LB(h)$) was set to 10 satellites launched per year. Setting a lower bound above zero prevents the optimizer from avoiding placing any satellites at higher altitudes, an optimal but unrealistic scenario. An upper bound is necessary for good performance in the optimization problem and was chosen to be a function of the static atmospheric density profile, i.e., $UB(h) = 10^{16} \cdot \rho(h)$, since the drag constitutes the primary sink acting on derelicts and debris and is stronger at low altitudes due to higher atmospheric density; thus, it naturally allows to place more satellites at lower altitudes with respect to higher altitudes. This choice helps to speed up the convergence of the optimizer and reduces computational time. In order to obtain a true optimized result, UB should not bind at any point in the simulation, as binding constraints to UB alter the optimization outcomes. $UB(h)$ does bind in simulations with low α_a and high P_M, but UB was not adjusted in these examples to avoid introducing a confounding variable into the sensitivity analysis.

The results of the sensitivity analysis are reported in Figs. 6, 7 and 8. Figs. 6 and 7 show the increase in the total number of satellites ($S + S_u$) at the final time of the analysis using the MOCAT-4S model with slotting ($\zeta = 1$) as compared to the MOCAT-4S without slotting ($\zeta = 0$) as a function of α_a and P_M. The figures show that varying the collision avoidance efficacy coefficient (α_a) impacts the benefits of slotting on the capacity. In particular, for $\alpha_a = 0.01$

the benefits of slotting results in about 15,000 more satellites, whereas for $\alpha_a = 0.1$ the benefits is about 125,000 more satellites. There is only a weak relationship with PMD percentage, which is expected, as P_M mostly affects the number of created derelicts, decreasing capacity similarly across different values of the P_M parameter.

When the collision avoidance failure coefficient is low, slotting directly helps to minimize collisions and debris generation, thus allowing for more satellites in orbit. Nevertheless, benefits appear to be minimal for realistic levels of collision avoidance efficacy (i.e. probably 10^{-3} and lower) and the parameters used in these simulations. Gains from slotting represent less than 1% of saturated orbital capacity for $\alpha_a = 10^{-2}$, and less for better collision avoidance levels.

Slotting offers another potential benefit in addition to greater capacity subject to a long-term sustainability constraint: improved spaceflight safety and reductions to the number of spacecraft lost to collisions. Fig. 8 shows the difference in the number of satellites lost per year at the final time step (τ_f) because of the collisions between active satellites considering slotting ($\zeta = 1$) and without slotting ($\zeta = 0$). For high values of α_a (worse collision avoidance efficacy), a lower number of satellites is destroyed if slotting is used. As an example, about 1,200 satellites are saved with slotting for $\alpha_a = 0.01$ and 11,000 for $\alpha_a = 0.1$. This reduces the need to replace satellites that get hit by debris (or over-provision constellations in anticipation of collision events), saving money and simplifying operations. While slotting requires additional up-front considerations during orbit design and cross-operator coordination, it does not impose substantial hardware or other costs on operators using it, meaning these benefits are largely "free". The number of satellites that slotting preserves is strongly dependent on collision avoidance efficacy.

In addition to the above benefits, slotting also offers potential operational benefits because it passively avoids cross-operator conjunctions, reducing the cadence of necessary collision avoidance maneuvers. While many operators try to incorporate such maneuvers into their regular station-keeping when possible and have well established workflows for collision avoidance, cross-operator coordination remains less than seamless and conjunction burdens will only increase as orbital density grows.

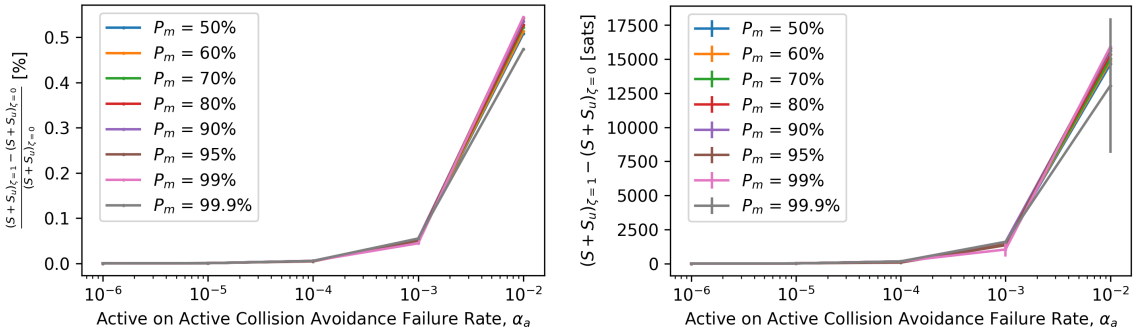

(a) Percentage

(b) Absolute Capacity

Fig. 6: Gain in capacity by using orbital slotting as a function of post-mission disposal success rate and collision avoidance failure rate $\in [10^{-6}, 10^{-2}]$.

5.1 Detailed Analysis for $\alpha_a = 0.01$ and $P_M = 95\%$

In this section, a detailed description is presented for the case where $\alpha_a = 0.01$ and $P_M = 95\%$. This example is used to better visualize and understand the optimal results, the predictions of the MOCAT-4S model, the computed capacity, as well as the benefits of including orbital slotting within the model. For this case, the best solution among multiple runs of the PSO is presented.

The computed optimal launch rate for slotted satellites is shown in Fig. 9. It can be observed that, apart from the higher altitudes where the minimum admissible launch rate is chosen by the optimizer to reduce high altitude debris creation, for the rest of the altitude regimes the optimized launch rate is very close or identical to the upper bound. This is related to what has been mentioned before that a compromise on the upper bound had to be carried out for the sensitivity analysis in order to make it convenient for all the possible cases. However, approaching the upper bound means that a higher capacity can eventually be obtained if a higher upper bound is set. This is also the reason why the sustainability constraint (i.e., the time derivative of the debris at final time) is never close to the imposed threshold, as

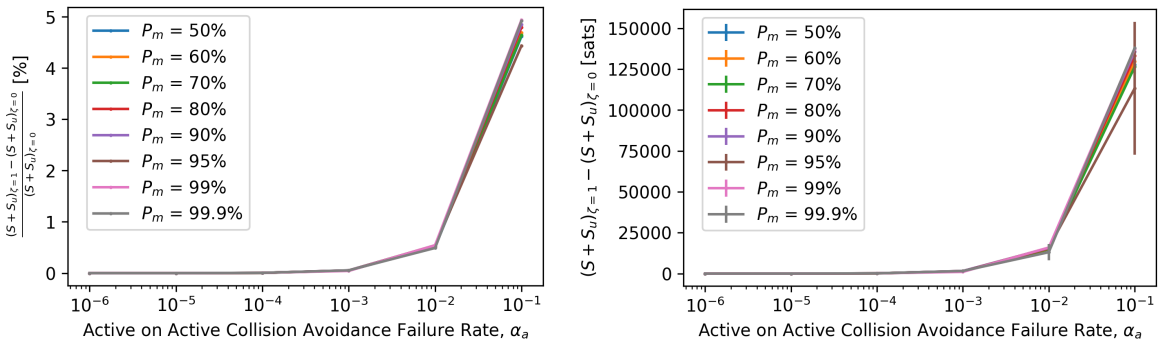

(a) Percentage

(b) Absolute Capacity

Fig. 7: Gain in capacity by using orbital slotting as a function of post-mission disposal success rate and collision avoidance failure rate $\in [10^{-6}, 10^{-1}]$.

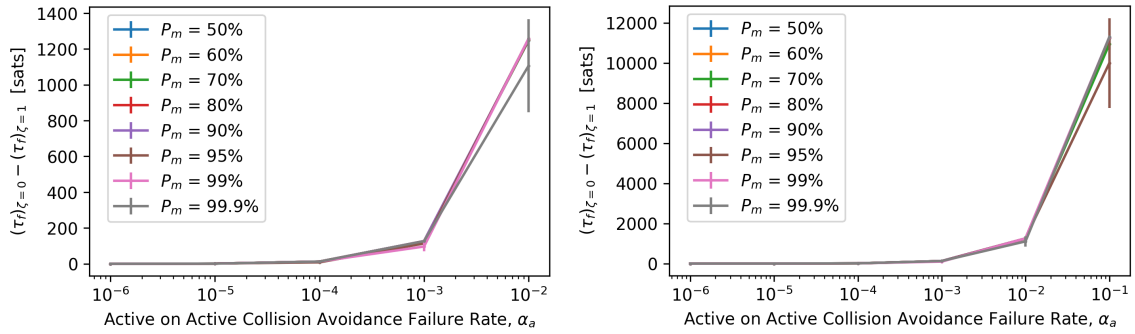

(a) Results up to $\alpha_a = 0.01$.

(b) Results up to $\alpha_a = 0.1$.

Fig. 8: Difference between the number of destroyed satellites at final time without slotting ($\zeta = 0$) and with slotting ($\zeta = 1$).

shown in the red dots of Fig. 10.

In the same figure, the blue dots, representing the available capacity within the intrinsic capacity constraint (Eq. (18)), show that the capacity is almost full at low altitudes, where capacity is higher. As altitude increases, there is still available intrinsic capacity, but overall capacity is potentially limited by the generation of new debris at altitudes where it is long-lived. This indicates that intrinsic capacity is the main constraint at lower altitudes, whereas the sustainability constraint becomes significant at higher altitudes. Since the time derivative of the debris constraint is never approached, even at high altitudes, this test case could be further optimized by increasing the upper bound of the launch rate, allowing the generation of more debris as long as generation remains under the imposed maximum level.

In this simulation, debris also decreases within the range 800-900 km. This is due to the combination of many aspects, including the slotting mechanism that reduces collisions, the sustainability constraint, and the minimal but non-zero atmospheric drag. The decreasing debris behaviour can also be appreciated, especially for high altitudes, in Fig. 11(b), which illustrates the debris species as a function of time and altitude. On the other hand, Fig. 11(a) shows an increase in the number of derelicts, due to the high amount of new satellites launched into orbit, with peaks in the range 350-550 km. This is the range where many satellites are launched, but at an altitude with only moderate drag effects.

The trend of the total orbital density, considering all the ASOs in orbit (including the slotted satellites) as a function of both altitude and time is plotted in Fig. 12. Most of the satellites, and resulting debris and derelicts are placed at low altitudes (200-400 km). The trend of the unslotted satellites population is not reported since it is very similar to the slotted satellites trend due to the assumptions of $\lambda_u(h) = \theta_{S,S_u}\lambda_s(h)$. Moreover, Fig. 13 reports the population as a function of time. It is possible to see that all the populations of ASOs quickly reach a plateau after a preliminary

transient. As expected, the debris population does not exhibit significant growth because of the imposed sustainability constraint. The computed optimal LEO capacity, subject to the proposed constraints, results in about 2.9 millions of satellites, divided into 2.64 millions of slotted and 0.26 millions of unslotted.

Finally, Fig. 14 reports the number of destroyed satellites due to the collisions (with all the other species) at the final time of the analysis with slotting (quantities with subscript 4) and without slotting (quantities with subscript 3). As already observed, slotting increases orbital capacity and reduces the number of collisions and debris, preventing the loss of numerous active satellites, as shown in the sensitivity analysis. These benefits are more evident at low altitudes where more slotted satellites can be launched due to higher atmospheric density and stronger drag effects on derelicts and debris. As already said, this results in economic advantages and cost savings.

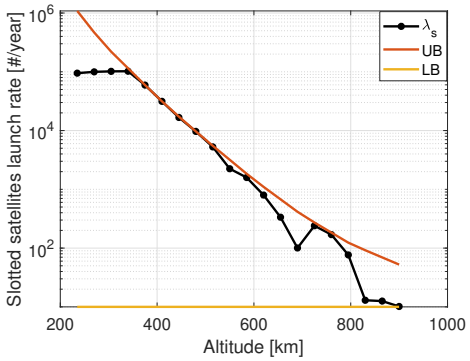

Fig. 9: Optimized launch rate.

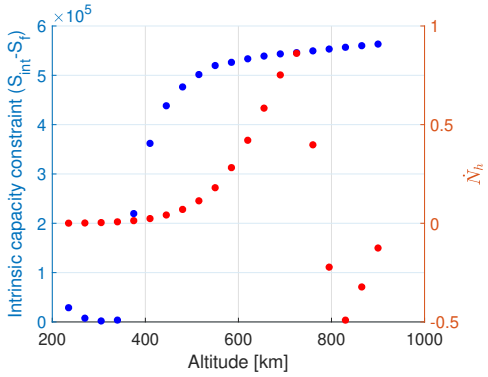

Fig. 10: Intrinsic capacity and sustainability constraints.

5.2 MOCAT-4S Simulation using ITU Slotted Shell Data as Initial Condition

The population of shells larger than 100 satellites in Section 2 was then used to augment the initial conditions derived from space-track.org for another sensitivity study in α_a and P_M.[1] The new updated initial population of slotted satellites is shown in Fig. 15. As can be seen, compared to Fig. 5, the initial slotted satellites population is much higher. However, most of the satellites are located at low altitudes, with the highest peaks around 550 and 650 km of altitude, respectively. According to Fig. 11 of [21], the residence time in LEO considering circular orbit and a static exponential density profile for an object with area-to-mass ratio of 0.01 m^2/kg (for the slotted satellites population in this paper the area-to-mass ratio is 0.0078 m^2/kg) is about 100 years at 700 km. This means that, since the propagation time chosen for this paper is 200 years, the initial population does not affect too much the capacity of LEO in the long term horizon. Indeed, for this kind of analysis, the final population will be similar to the launch rate profile chosen by the optimizer. To perform the sensitivity analysis, because this population would probably exceed the constraints used in

[1] Satellite associated with these ITU filings that are already on-orbit (mostly from Starlink) are double-counted by this approach, but the number of double-counted satellites is small relative to the overall demand profile.

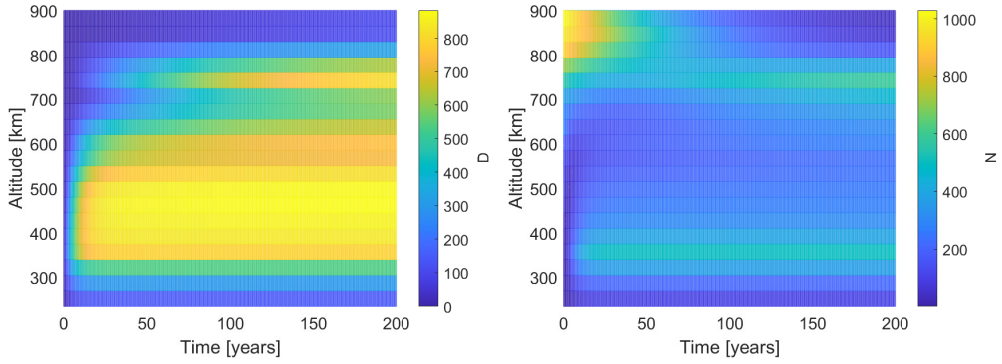

(a) Derelicts. (b) Debris.

Fig. 11: Initial and final distribution of derelicts and debris.

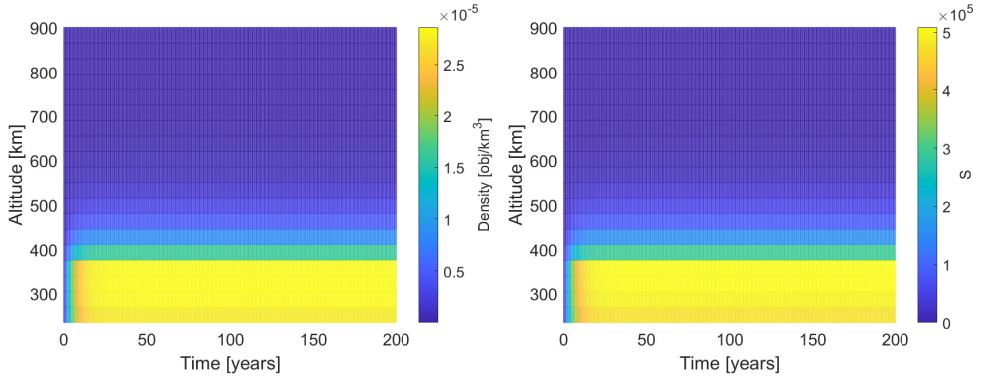

(a) Total orbital density. (b) Slotted satellites density.

Fig. 12: Density vs time and altitude.

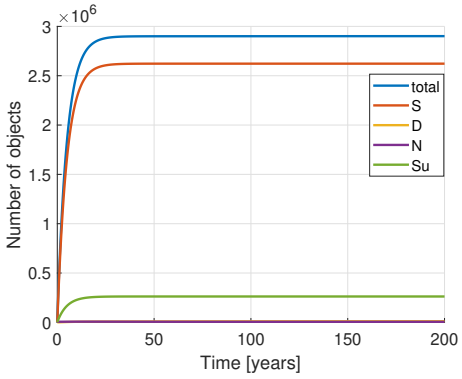

Fig. 13: ASOs population over time.

the previous sensitivity study, the number of admissible debris objects produced per year was increased to 30. All the other parameters as well as the lower and upper bound of the launch rate are the same of the previous analysis. Results are excluded for $P_m = 0.5$, as the optimizer was unable to generate compliant solutions for the ITU initial conditions. Indeed, the higher population of satellites generate more derelicts and thus more collisions and debris in the short term horizon, overcoming the imposed sustainability constraint. As can be seen in Figs. 16 and 17, the results appear quite similar to Figs. 6(b), 7(b) and 8. The same considerations made previously are still valid for this case. The similarities

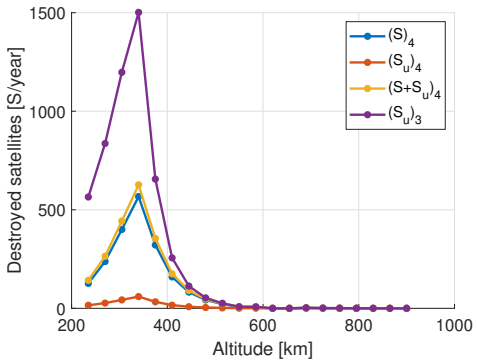

Fig. 14: Satellites destroyed per year at the final time of the propagation.

are due to what has been said before related to the effect of the initial population on the capacity just on the short term horizon and not on the long term, for which the propagation time is long enough to make the remains of the initial population of slotted satellites in terms of derelicts and debris deorbit and re-enter.

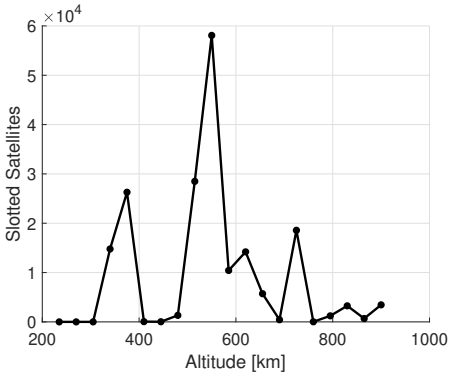

Fig. 15: Updated initial population of slotted satellites considering ITU.

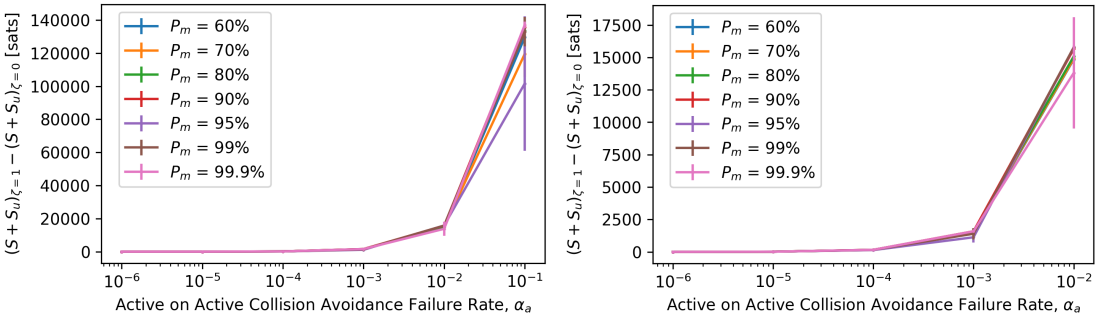

(a) Results up to $\alpha_a = 0.1$.

(b) Results up to $\alpha_a = 0.01$.

Fig. 16: Gains to capacity with ITU initial conditions

6. CONCLUSIONS

This paper proposed a new approach to combine orbital slotting with a multi-species multi-bin source-sink model, called MOCAT-4S. The model was propagated with an optimization technique, based on the PSO, to estimate the

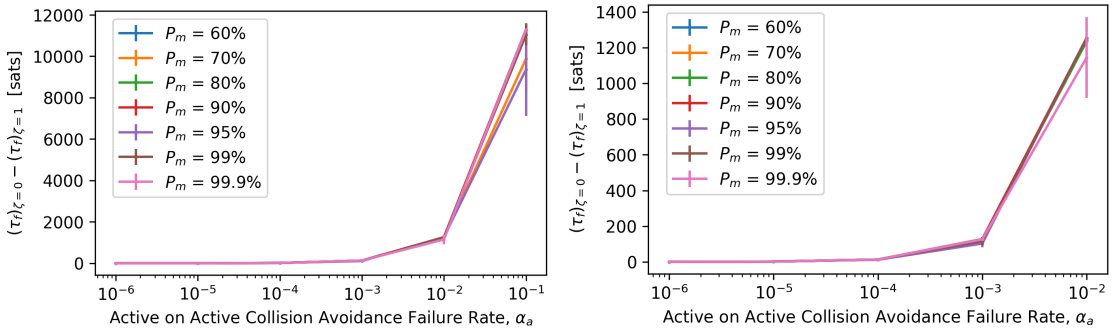

(a) Results up to $\alpha_a = 0.1$.

(b) Results up to $\alpha_a = 0.01$.

Fig. 17: Avoiding active on active satellite collisions with ITU initial conditions

LEO orbital capacity subject to different constraints. These constraints include an intrinsic capacity constraint, related to the maximum number of slotted satellites admissible per altitude bin in order to indefinitely maintain a minimum separation distance, and sustainability constraints on levels of acceptable net debris change. A grid search study was performed to examine the benefits of LEO slotting for various levels of active on active collision avoidance efficacy and post-mission disposal compliance for both present day initial conditions and those associated with demand drawn from LLC filings at the ITU. Results demonstrate that slotting tends to provide only limited gains to orbital capacity for low values of collision avoidance failure rate (10^{-3} and lower), which means better collision avoidance, but it is still very useful since it may avoid enough active on active collisions to motivate adoption for short-term safety of flight and space traffic management reasons.

Future works will further investigate the reasons for the results obtained in these sensitivity analyses, including altitude-dependent rather than absolute changes to capacity and collision risk. Similarly, sensitivity will be explored subject to economic sustainability constraints associated with the maximum acceptable levels of active satellite collisions. Furthermore, a follow-up study will consider the higher LEO altitude regimes, where debris objects are much longer lived.

A parallel stream of work will compare MOCAT models against other existing models using different modeling approaches to assess the level of precision and accuracy associated with the source-sink methodology as implemented.

ACKNOWLEDGEMENTS

The authors acknowledge the MIT SuperCloud and Lincoln Laboratory Supercomputing Center for providing high performance computing resources that have contributed to the research results reported within this paper. They thank Thomas Roberts for sharing processed ITU filing data. This work is sponsored by the Defense Advanced Research Projects Agency (Grant N66001-20-1-4028), and the content of the information does not necessarily reflect the position or the policy of the Government. No official endorsement should be inferred. Distribution statement A: Approved for public release; distribution is unlimited.

REFERENCES

[1] David Arnas, Miles Lifson, Richard Linares, and Martín E Avendaño. Definition of Low Earth Orbit slotting architectures using 2D lattice flower constellations. *Advances in Space Research*, 67(11):3696–3711, jun 2021.

[2] Miles Lifson, David Arnas, and Richard Linares. Low Earth Orbit Slotting: Implications for Orbit Design and Policy. In International Academy of Astronautics, editor, *8th Annual Space Traffic Management Conference*, pages 1–23, Austin, TX, 2022.

[3] Andrea D'Ambrosio, Miles Lifson, and Richard Linares. The capacity of low earth orbit computed using source-sink modeling. *arXiv*, 2022.

[4] Andrea D'Ambrosio, Simone Servadio, Peng Mun Siew, Daniel Jang, Miles Lifson, and Richard Linates. Analysis of the LEO orbital capacity via probabilistic evolutionary model. In *2022 AAS/AIAA Astrodynamics Specialist Conference, Charlotte, North Carolina, August 7-11*, 2022.

[5] Donald J Kessler and Burton G Cour-Palais. Collision frequency of artificial satellites: The creation of a debris belt. *Journal of Geophysical Research: Space Physics*, 83(A6):2637–2646, 1978.

[6] Donald J. Kessler and Phillip D. Anz-Meador. Critical number of spacecraft in low earth orbit: Using satellite fragmentation data to evaluate the stability of the orbital debris environment. *European Space Agency, (Special Publication) ESA SP*, 1(473):265–272, 2001.

[7] Donald J Kessler, Nicholas L Johnson, JC Liou, and Mark Matney. The kessler syndrome: implications to future space operations. *Advances in the Astronautical Sciences*, 137(8):2010, 2010.

[8] David L Talent. Analytic model for orbital debris environmental management. *Journal of spacecraft and rockets*, 29(4):508–513, 1992.

[9] Gian Luigi Somma, Camilla Colombo, HG Lewis, et al. A statistical leo model to investigate adaptable debris control strategies. In *7th European Conference on Space Debris, ESA/ESOC*, pages 1–12. ESA, 2017.

[10] Gian Luigi Somma. *Adaptive remediation of the space debris environment using feedback control*. PhD thesis, University of Southampton, 2019.

[11] V Trozzi, C Colombo, and M Trisolini. Analysis of possible definitions of the space environment capacity to pursue long-term sustainability of space activities. In *72nd International Astronautical Congress (IAC 2021)*, pages 1–14, 2021.

[12] Miles Lifson, David Arnas, Martin Avendaño, and Richard Linares. A Method for Generating Closely Packed Orbital Shells and the Implication on Orbital Capacity. 2022.

[13] Miles Lifson, Andrea D'Ambrosio, David Arnas, and Richard Linares. How Many Satellites Can We Fit in Low Earth Orbit?: Capacity integrating Risk-based and Intrinsic Methods. In *2022 AAS/AIAA Astrodynamics Specialist Conference, Charlotte, North Carolina, August 7-11*, 2022.

[14] ITU e-submission of satellite network filings. `https://www.itu.int/ITU-R/space/asreceived/`.

[15] David A Vallado. *Fundamentals of Astrodynamics and Applications*, volume 4th edn. Edited by T. S. T. Library. Hawthorne, CA: Microcosm Press and Springer, 2013.

[16] PH Krisko. Proper implementation of the 1998 nasa breakup model. *Orbital Debris Quarterly News*, 15(4):1–10, 2011.

[17] M. Avendaño, D. Arnas, R. Linares, and M. Lifson. Efficient Search of Optimal Flower Constellations. In *Proceedings of the 71st International Astronautical Congress (IAC)*. International Astronautical Federation, 2020.

[18] Martín Avendaño, David Arnas, Richard Linares, and Miles Lifson. Efficient search of optimal Flower Constellations. *Acta Astronautica*, 179:290–295, feb 2021.

[19] David Arnas and Richard Linares. Non-self-intersecting trajectories and their applications to satellite constellation design and orbital capacity. 2021.

[20] Albert Reuther, Jeremy Kepner, Chansup Byun, Siddharth Samsi, William Arcand, David Bestor, Bill Bergeron, Vijay Gadepally, Michael Houle, Matthew Hubbell, Michael Jones, Anna Klein, Lauren Milechin, Julia Mullen, Andrew Prout, Antonio Rosa, Charles Yee, and Peter Michaleas. Interactive supercomputing on 40,000 cores for machine learning and data analysis. In *2018 IEEE High Performance extreme Computing Conference (HPEC)*, pages 1–6. IEEE, 2018.

[21] Matthew Stevenson, Darren McKnight, Hugh Lewis, Chris Kunstadter, and Rachit Bhatia. Identifying the statistically-most-concerning conjunctions in leo. In *2021 Advanced Maui Optical and Space Surveillance Technologies Conference (AMOS), Maui, Hawaii*, 2021.

APPENDIX

Table 5: LLCs Shells In ITU Filings (200-900 km, >100 satellites/shell, Rwandan LLCs excluded, circular orbits only, clear duplicates removed)

Submission Reference Number	Operating Agency	Satellite Name	Altitude (km)	Inclination (deg)	Number of Satellites
D2021-37348	SWARM TECHNOLOGIES	ASTROBIENE	325.0	97.6	144
D2021-37348	SWARM TECHNOLOGIES	ASTROBIENE	325.0	97.4	150
D2021-37348	SWARM TECHNOLOGIES	ASTROBIENE	325.0	45.0	120
USA2019-23661	SPACE EXPLORATION TECHNOLOGIES CORP.	USASAT-NGSO-3W-1	328.3	30.0	3,000
USA2019-23657	SPACE EXPLORATION TECHNOLOGIES CORP.	USASAT-NGSO-3V-1	334.4	40.0	3,000
D2021-42541	New operating agency	MARS-E1	340.0	53.0	10,560
D2021-42541	New operating agency	MARS-E1	345.0	46.0	10,560
USA2019-23653	SPACE EXPLORATION TECHNOLOGIES CORP.	USASAT-NGSO-3U-1	345.6	53.0	3,000
D2021-42541	New operating agency	MARS-E1	350.0	38.0	10,560
D2021-42541	New operating agency	MARS-E1	360.0	96.9	7,200
USA2017-01700	PLANET LABS PBC	USASAT-30F	475.0	97.3	180
USA2019-23647	SPACE EXPLORATION TECHNOLOGIES CORP.	USASAT-NGSO-3T-1	482.8	30.0	3,000
D2020-36222	New operating agency	D-NGSO-1120-2	485.0	55.0	1,260
USA2019-23641	SPACE EXPLORATION TECHNOLOGIES CORP.	USASAT-NGSO-3S-1	488.4	40.0	3,000
USA2019-23635	SPACE EXPLORATION TECHNOLOGIES CORP.	USASAT-NGSO-3R-1	498.8	53.0	3,000
F2020-34105	MINISTERE DE LA DEFENSE	FMS-LEO	500.0	50.0	1,296
F2020-34105	MINISTERE DE LA DEFENSE	FMS-LEO	500.0	85.0	1,296
E2021-39976	EMACON	SECOMSAT-LEO-1	500.0	97.4	3,600
USA2021-44033	LYNK GLOBAL, INC.	USASAT-NGSO-10	500.0	53.0	4,910
E2021-37456	HISPASAT, S.A.	HISPASAT-LEO-BB-2	500.0	97.4	552
CHN2020-33636	CHINA TELECOM SATELLITE COMMUNICATIONS	GW-A59	508.0	55.0	3,600
USA2019-23633	SPACE EXPLORATION TECHNOLOGIES CORP.	USASAT-NGSO-3Q	517.8	70.0	3,000
F2019-24239	EUTELSAT SA	F-SAT-NG-11	520.0	86.0	405
E2021-37456	HISPASAT, S.A.	HISPASAT-LEO-BB-2	520.0	54.5	1,638
F2019-24239	EUTELSAT SA	F-SAT-NG-11	520.0	52.0	270
E2021-39976	EMACON	SECOMSAT-LEO-1	520.0	80.0	3,600
E2021-39976	EMACON	SECOMSAT-LEO-1	520.0	30.0	3,600
E2021-39976	EMACON	SECOMSAT-LEO-1	520.0	53.5	3,600
USA2019-23631	SPACE EXPLORATION TECHNOLOGIES CORP.	USASAT-NGSO-3P	524.7	75.0	3,000
D2021-42541	New operating agency	MARS-E1	525.0	53.0	6,720
D2021-42541	New operating agency	MARS-E1	527.5	43.0	3,360
D2021-44554	STARLINK GERMANY GMBH	MARS-K1	527.5	43.0	1,680
D2021-42541	New operating agency	MARS-E1	530.0	43.0	6,720

USA2019-23629	SPACE EXPLORATION TECHNOLOGIES CORP.	USASAT-NGSO-3O	532.0	80.0	3,000
D2021-42541	New operating agency	MARS-E1	535.0	33.0	6,720
USA2019-23625	SPACE EXPLORATION TECHNOLOGIES CORP.	USASAT-NGSO-3N	539.7	85.0	3,000
D2021-42541	New operating agency	MARS-E1	540.0	53.2	1,584
USA2021-42315	FEDERAL COMMUNICATIONS COMMISSION - SD	USASAT-NGSO-3D	540.0	53.2	1,512
NOR2021-36940	STEAM SYSTEMS A/S	STEAM-1	540.0	53.2	1,584
NOR2021-36940	STEAM SYSTEMS A/S	STEAM-1	550.0	53.0	3,168
NOR2021-42410	STEAM SYSTEMS A/S	STEAM-2B	550.0	53.0	3,168
NZL2019-20766	PRIVATE	SNZL-NGSO-1	550.0	50.0	216
USA2019-13393	SPACE EXPLORATION TECHNOLOGIES CORP.	USASAT-NGSO-3A-R	550.0	53.0	1,584
USA2021-44033	LYNK GLOBAL, INC.	USASAT-NGSO-10	550.0	97.0	200
D2021-42541	New operating agency	MARS-E1	550.0	53.0	1,584
NOR2021-36942	STEAM SYSTEMS A/S	STEAM-2	560.0	97.6	520
NOR2021-36940	STEAM SYSTEMS A/S	STEAM-1	560.0	97.6	520
D2021-42541	New operating agency	MARS-E1	560.0	97.6	520
NOR2021-36942	STEAM SYSTEMS A/S	STEAM-2	570.0	70.0	720
NOR2021-36940	STEAM SYSTEMS A/S	STEAM-1	570.0	70.0	720
D2021-42541	New operating agency	MARS-E1	570.0	70.0	720
CAN2018-02154	KEPLER COMMUNICATIONS INC.	KELYPSIS	575.0	97.7	175
USA2019-23627	SPACE EXPLORATION TECHNOLOGIES CORP.	USASAT-NGSO-3M	580.0	97.7	1,500
D2021-37348	SWARM TECHNOLOGIES	ASTROBIENE	585.0	97.6	144
D2021-37348	SWARM TECHNOLOGIES	ASTROBIENE	585.0	97.4	186
CHN2020-33636	CHINA TELECOM SATELLITE COMMUNICATIONS	GW-A59	590.0	85.0	480
D2020-34001	New operating agency	KBSAT-NGSO-1	590.0	33.0	784
USA2019-12909	KUIPER SYSTEMS LLC	USASAT-NGSO-8C	590.0	33.0	784
F2020-34105	MINISTERE DE LA DEFENSE	FMS-LEO	600.0	85.0	1,152
F2020-33408	EUTELSAT SA	F-SAT-NG-14	600.0	89.5	1,104
F2020-34105	MINISTERE DE LA DEFENSE	FMS-LEO	600.0	50.0	1,152
F2020-33408	EUTELSAT SA	F-SAT-NG-14	600.0	51.0	1,104
F2019-26189	ONEWEB LTD	VERITY	600.0	55.0	1,152
D2020-36222	New operating agency	D-NGSO-1120-2	600.0	55.0	900
CHN2020-33636	CHINA TELECOM SATELLITE COMMUNICATIONS	GW-A59	600.0	50.0	2,000
D2021-42541	New operating agency	MARS-E1	604.0	148.0	288
D2020-34001	New operating agency	KBSAT-NGSO-1	610.0	42.0	1,296
USA2019-13020	KUIPER SYSTEMS LLC	USASAT-NGSO-8B	610.0	42.0	1,296
D2021-42541	New operating agency	MARS-E1	614.0	115.7	648
PNG2021-39760	OMNISPACE LLC	UHF-TTC-L2	630.0	98.0	144
D2020-34001	New operating agency	KBSAT-NGSO-1	630.0	51.9	1,156
USA2019-12905	KUIPER SYSTEMS LLC	USASAT-NGSO-8A	630.0	51.9	1,156
D2021-39267	AMAZON DEVELOPMENT CENTER GERMANY GMBH	KBSAT-NGSO-P	650.0	74.0	651
D2021-39267	AMAZON DEVELOPMENT CENTER GERMANY GMBH	KBSAT-NGSO-P	650.0	76.0	650
D2021-39267	AMAZON DEVELOPMENT CENTER GERMANY GMBH	KBSAT-NGSO-P	650.0	78.0	652

D2021-39267	AMAZON DEVELOPMENT CENTER GERMANY GMBH	KBSAT-NGSO-P	650.0	72.0	652
D2021-39267	AMAZON DEVELOPMENT CENTER GERMANY GMBH	KBSAT-NGSO-P	650.0	80.0	650
F2019-24239	EUTELSAT SA	F-SAT-NG-11	680.0	86.0	216
PNG2018-05811	OTHERS NOT SHOWN ON ABOVE (B) LIST	MICRONSAT	698.0	85.0	105
D2020-36222	New operating agency	D-NGSO-1120-2	700.0	55.0	720
F2020-34105	MINISTERE DE LA DEFENSE	FMS-LEO	700.0	85.0	1,088
E2021-39976	EMACON	SECOMSAT-LEO-1	700.0	80.0	3,600
E2021-37456	HISPASAT, S.A.	HISPASAT-LEO-BB-2	700.0	53.5	1,056
E2021-39976	EMACON	SECOMSAT-LEO-1	700.0	53.5	3,600
F2020-34105	MINISTERE DE LA DEFENSE	FMS-LEO	700.0	50.0	1,088
E2021-39976	EMACON	SECOMSAT-LEO-1	700.0	30.0	3,600
E2021-37456	HISPASAT, S.A.	HISPASAT-LEO-BB-2	720.0	98.3	400
E2021-39976	EMACON	SECOMSAT-LEO-1	720.0	98.3	3,600
CHN2020-33355	ZHEJIANG GEESPACE TECHNOLOGY CO., LTD.	GEESAT-JL	800.0	50.0	132
E2021-39976	EMACON	SECOMSAT-LEO-1	800.0	88.0	540
E2021-39976	EMACON	SECOMSAT-LEO-1	800.0	90.0	720
F2019-14212	AIRBUS DEFENCE & SPACE	AST-NG-NC-1B	800.0	88.0	180
F2021-36734	THALES ALENIA SPACE	MCSAT-2 LEO-2	800.0	90.0	288
F2020-34105	MINISTERE DE LA DEFENSE	FMS-LEO	800.0	50.0	960
F2020-34105	MINISTERE DE LA DEFENSE	FMS-LEO	800.0	85.0	960
G2021-44278	MANSAT LIMITED	SN-CONSTELLATION1	830.0	55.0	1,190
CHN2018-09429	BEIJING XINWEI TECHNOLOGY CO. LTD	TXIN-WB	850.0	86.0	109
CHN2018-02590	SPACE INTEGRATED GROUND INFORMATION NETWORK CO. LTD.	SIGNSAT-NGSO	880.0	86.0	239
F2019-14212	AIRBUS DEFENCE & SPACE	AST-NG-NC-1B	900.0	88.0	1,092
F2020-33408	EUTELSAT SA	F-SAT-NG-14	900.0	89.5	1,104
E2021-39976	EMACON	SECOMSAT-LEO-1	900.0	88.0	1,260
F2020-34105	MINISTERE DE LA DEFENSE	FMS-LEO	900.0	50.0	840
F2020-33408	EUTELSAT SA	F-SAT-NG-14	900.0	51.0	1,104
F2020-34105	MINISTERE DE LA DEFENSE	FMS-LEO	900.0	85.0	840